Maciej ŁUSZCZEK, Grzegorz ŁUSZCZEK, Dariusz ŚWISULSKI

Gdańsk University of Technology, Faculty of Electrical and Control Engineering

doi: 10.15199/48.2021.05.17

Simulation investigation of perovskite-based solar cells

Abstract. *Three models of thin-layer lead-halide perovskite solar cells with different electron-transport layers (TiO_2, SnO_2, ZnO) were investigated by the simulation method. The perovskite layer thickness was optimized for all the systems. The analysis of the standard photovoltaic cell performance parameters at various operating temperatures was performed. The best performance was achieved for the system with the SnO_2 conductive layer.*

Streszczenie. *Przeprowadzono badania symulacyjne trzech modeli ołowiowo-halogenkowych perowskitowych ogniw słonecznych z różnymi warstwami odpowiedzialnymi za transport elektronowy (TiO_2, SnO_2, ZnO). Dla wszystkich układów dokonano optymalizacji grubości warstwy perowskitu. Przeanalizowano standardowe parametry określające wydajność ogniw fotowoltaicznych w różnych temperaturach pracy. Największą sprawność uzyskano dla układu z warstwą przewodzącą SnO_2.* ***(Badania symulacyjne perowskitowych ogniw słonecznych)***

Keywords: perovskite, solar cell, simulation, drift-diffusion model, operating temperature
Słowa kluczowe: perowskit, ogniwa słoneczne, symulacje, model dryfowo-dyfuzyjny, temperatura pracy

Introduction

Perovskite solar cells (PSC) seem to be a very promising alternative for conventional solutions available on the photovoltaic market, mainly because of their ability to absorb wide spectrum of the sunlight, high power conversion efficiencies (PCE) and potentially low costs of mass production. What is more, PSC could be very thin, flexible, transparent and light-weighted, what opens up many applications for this class of novel photovoltaic devices.

There are, in principle, two types of constructions utilized for the perovskite photovoltaic device preparation: a normal structure or an inverted structure. The both architectures contains perovskite layer (absorber), transparent electrodes made of conductive materials, typically fluorine-doped tin oxide (FTO) or indium tin oxide (ITO), electron transport layers (ETL), hole-transport layers (HTL) and metal contacts, as it is depicted in Fig. 1. The perovskite material exhibits characteristic ABX_3 crystal structure, where: A — organic cation (CH_3NH_3, NH_2CHNH_2), B — metalic cation (Pb, Sn), X — halide anion (I, Br, Cl). Although various organic compounds are intensively tested as conductive layers, there are also some promising conductive inorganic semiconductors to be used as ETL (e.g. TiO_2, ZnO, SnO_2, In_2O_3) and HTL (e.g. NiO_x, CuI, Cu_2O, $CuSCN$) materials.

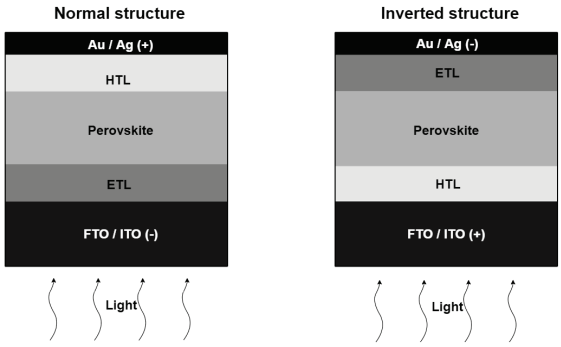

Fig. 1. Normal and inverted structures of perovskite solar cells

Despite many unquestionable advantages, perovskite solar cell technology is still under intensive development aimed to commercialization in the nearest future. Researchers try to increase efficiency and stability of perovskite photovoltaic devices, as well as to prolong the lifetime, e.g. by adding additional interlayers, optimizing thickness of active layers or modifying their physical properties during the technological process of fabrication. Various physical parameters of individual layers of the perovskite-based solar cells, such as: band gap, electron affinity, relative permittivity, electron and hole mobilities, concentrations of donors and acceptors, deep-level defect concentration and many others, can significantly influence the light conversion efficiency.

The aim of this article is to present simulation results of thin-film lead-halide perovskite solar cells with different inorganic transparent conductive oxides used as charge transport layers. The power conversion efficiency (PCE), fill factor (FF), open-circuit voltage (V_{oc}), short-circuit current (J_{sc}) and output cell power were analyzed for selected series and shunt resistances. The temperature effect on the overall device performance was also examined.

Physical foundations

In general, all photovoltaic devices (PV) involve a semiconducting material to absorb the light (photons) and conduct the as-generated charge carriers. The working principle of various PV can differ in details, but there are some fundamental effects included, which are common. The absorption of photon occurs, when its energy, $E_{ph} = h\nu$, is equal or grater than the semiconductor's energy band gap, E_g, and leads to the promotion of an electron (e^-) from the valence band (VB) to the conduction band (CB), what is known as an internal photoelectric effect (see Fig. 2). As a result, an electronic vacancy in the valence band, a hole (h^+), is created. The electron and the hole are attracted to each other by the electrostatic Coulomb force giving an electrically neutral quasiparticle called exciton. To generate free carriers, which are capable to transport the charge through the semiconductor, the electron and the hole have to be "disconnected" during the exciton dissociation process. Now, the electron and hole carriers are free to move separately and they could diffuse in the opposite directions.

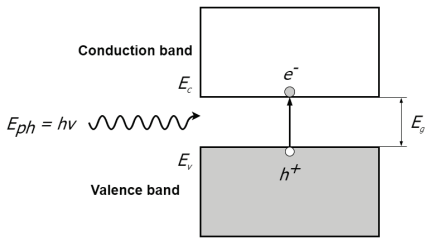

Fig. 2. Schematic representation of the internal photoelectric effect

An effective spatial separation of the photo-generated carriers is possible when the PV device is configured as a n-p (or p-n) junction. When electrons, being the majority carriers in the n-type semiconductor, diffuse across the junction from the n-side (high electron concentration) into the p-side (low electron concentration), they recombine with holes.

Analogously, holes (majority carriers) move from the p-type region into the n-type region of the junction and recombine with electrons. As a consequence, a diffusion current is generated and a zone, commonly known as a depletion region or a space charge region, is formed, where there are practically no mobile electrons and holes but there are ionized acceptors on the p-side and ionized donors on the n-side, instead. In this way, the internal (built-in) electric field appears, which, on the contrary to the diffusion, makes minority carriers flowing in the opposite directions, that is, the electrons move from the p-side into the n-side and the holes move from the n-side into the p-side. This effect is responsible for the so-called drift current, flowing in an opposite direction to the current in a forward-biased diode. When the electron-hole pair is generated by the photon in the depletion region, the strong built-in electric field push the electron toward the n-region and the hole toward the p-region of the device (reverse current). On the other hand, outside the depletion region the electric field is weaker, thus the excess photo-generated electrons and holes participate mainly in the diffusion process. However, after reaching the junction the electrons from the p-side are "collected" and pushed toward the other side (n-region) and the same effect is observed for the holes from the n-side, which are moved toward the p-region. One can easily notice that the distribution of the charge carriers in the whole system depends strictly on a dynamic equilibrium between reverse and forward currents. In thin-film photovoltaic cells the diffusion of the carriers is reduced due to the existence of different kinds of defects, so the drift current is dominant. In other words, the built-in electric field extends practically to the whole thickness of the device. In the case of the PSC, n-i-p (normal structure) and p-i-n (inverted structure) architectures, containing an intrinsic perovskite layer, are used (see Fig. 3). These configurations enable the presence of the electric field in the entire i-region and thus the effectiveness of the charge transport in the photovoltaic device can be enhanced.

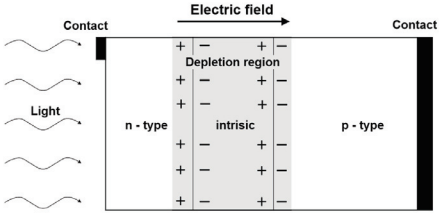

Fig. 3. Spatial charge distribution in the n-i-p junction of the solar cell

Another important issue to be carefully analyzed during the solar cell engineering is the band structure dissimilarity of semiconducting materials forming the interface (heterojunction). The differences of the energy band gaps of two semiconductors, E_{g1} and E_{g2}, as well as the unequal values of electron affinities, χ_1 and χ_2, which are defined in relation to the vacuum energy level, E_{vac}, lead to some offsets of the conduction and valence bands, ΔE_c and ΔE_v, respectively, and influence the transport of charge carriers. An example of band diagram of the heterojunction in the equilibrium conditions (short-circuit configuration) with the Fermi level, E_F, being constant along the whole structure is shown in Fig. 4 (left). The visible energy barrier qV_{bi} (q denotes the elementary charge) corresponds to the diffusion potential, V_{bi}, generated by the built-in electric field mentioned before (see Fig. 3). When the solar cell is in the open-circuit configuration, $V_{oc} = (E_{F2} - E_{F1})/q$ voltage appears (E_{F1}, E_{F2} are quasi Fermi levels) as it is presented in Fig. 4 (right).

As a rule of thumb, the better the band alignment, the higher the open-circuit voltage could be generated by the PV device.

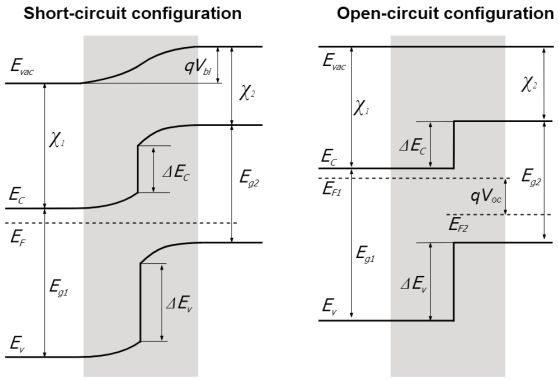

Fig. 4. Band diagram of a n-p heterojunction for short-circuit and open-circuit configurations

And last but not least, the behavior of a solar cell could be very well described by an equivalent circuit model containing discrete ideal electrical elements, namely, a current source in parallel with a diode (see Fig. 5). Because of the imperfectness of the real solar cell, a shunt resistance, R_{SH}, and a series resistance, R_S, should be taken into consideration. The output current, I, produced by the solar cell is equal: $I = I_L - I_D - I_{SH}$, where: I_L — photogenerated current, I_D — diode current, I_{SH} — shunt current.

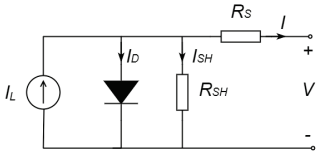

Fig. 5. Equivalent circuit of a photovoltaic cell

Simulation details

All simulations were performed using Solar Cell Capacitance Simulator (SCAPS-1D) software [2, 3], based on such fundamental approaches as the Poisson equation, the drift-diffusion model and the continuity equations, which are commonly exploited by the semiconductor theorists.

In this work three models of perovskite solar cells with $CH_3NH_3PbI_3$ perovskite sandwiched between CuI (HTL) and alternately TiO_2, SnO_2 or ZnO (ETL) layers in the n-i-p configuration (the normal structure), which is preferably used for thin-film PV devices, were investigated. Hereafter, these models are denoted as follows: Model 1 ($CuI/CH_3NH_3PbI_3/TiO_2$), Model 2 ($CuI/CH_3NH_3PbI_3/SnO_2$) and Model 3 ($CuI/CH_3NH_3PbI_3/ZnO$). It is worth to note, that the $CH_3NH_3PbI_3$ compound is probably the most popular PCS material, which can be fabricated by the spin-coating low cost process. On the other hand, the CuI hole-transport material exhibits good chemical stability and it can be easily deposited on various substrates at low temperatures by a relatively cheap method. Although TiO_2 is mostly used as an electron-transport layer in the n-i-p PCS, there are two other promising oxides to be regarded as ETL, that is, SnO_2 with better band alignment (see Fig. 6) or ZnO with higher conductivity. Noteworthy, the SnO_2 exhibits improved stability under ultraviolet (UV) illumination [4].

The parameters used for the simulations were taken from the literature [5, 6] and are collected in Table 1. The illumination source was assumed to be a standard solar spectrum AM 1.5G (1000 W/m^2). The calculations were per-

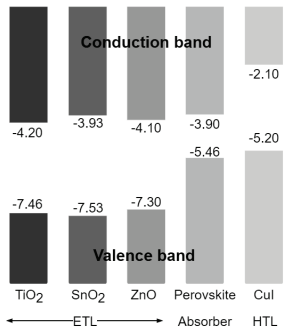

Fig. 6. Simplified band alignment diagram of the examined layers (numbers in electron-volt units—see Table 1)

formed using default SCAPS generation and absorption models, and a defect-originated Shockley-Read-Hall recombination (SRH) model. In this study the radiative band-to-band and Auger recombination mechanisms were neglected. To make the simulations more reliable the bulk defect densities in ETL i HTL were set up relatively high (10^{17} cm^{-3}). It is well known, that series resistance (R_S) and shunt resistance (R_{SH}) depend strongly on the fabrication method. Therefore, in the present work two scenarios were compared: a standard perovskite solar cell with R_S = 8.8 Ωcm^2 and R_{SH} = 337 Ωcm^2 [7] and an improved one with R_S = 3.0 Ωcm^2 and R_{SH} = 4250 Ωcm^2 [8].

Results

As a first step, the absorber (perovskite) layer thickness influence on the PSC performance was analyzed in the range of 0.2–1.0 μm with the rest of the parameters being unchanged. At the same time, the HTL and ETL thicknesses remained constant (0.2 μm). The simulated power conversion efficiency and fill factor as a function of perovskite thickness are presented in Fig. 7 and Fig. 8, respectively. One can notice from Fig. 6 that the PCE maximum appears at ∼0.50 μm, when TiO_2 is used as ETL (Model 1), and ∼0.45 μm for SnO_2 and ZnO (Models 2 and 3). The FF decreases with thickness of the perovskite layer due to the increase of the series resistance (Fig. 7). All essential performance parameters of the investigated devices after the thickness optimization are listed in Table 2. It is visible that the open-circuit voltage, V_{oc}, decreases with increasing thickness. On the other hand, for thicker perovskite layer the short-circuit density of current, J_{sc}, increases because of the enhanced absorption of the incident light. It was found that the best PSC performance (PCE = 18.33%, FF = 71.86%) could be achieved for the system with SnO_2 as the electron-transport layer. This effect could be explained by a very good band alignment of tin oxide and $CH_3NH_3PbI_3$, as schematically shown in Fig. 6. Among all the examined ETL materials the smallest CB band offset, ΔE_c = 0.03 eV, appears for the SnO_2–perovskite heterojunction, whereas the largest one (0.3 eV) is generated for the TiO_2–perovskite heterojunction. Because V_{oc} depends directly on the separation between the quasi Fermi levels, E_{Fn} and E_{Fp}, the negligible band offset results in stronger separation between E_{Fn} and E_{Fp}, what leads to higher open-circuit voltage in the PSC and, consequently, the FF improvement is achieved, too. The J-V characteristics obtained for the optimal thickness of the perovskite layer in all the investigated models are presented in Fig. 9. The simulation results are in good agreement with the experimental data for similar PSC devices [4, 7].

The operating temperature is one of the most important

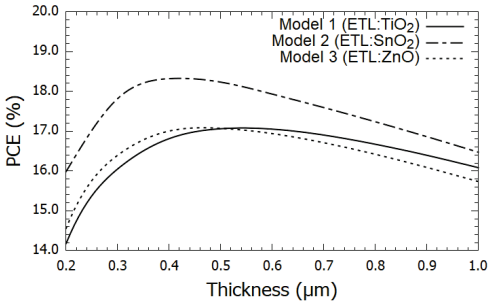

Fig. 7. Power conversion efficiency as a function of perovskite layer thickness

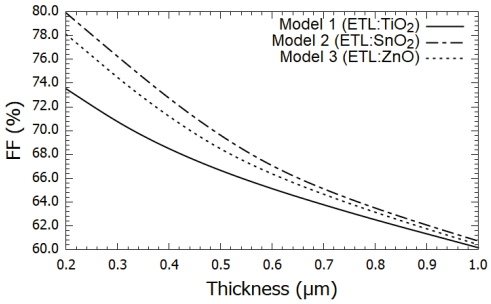

Fig. 8. Fill factor as a function of perovskite layer thickness

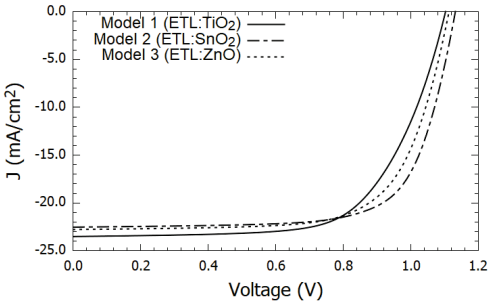

Fig. 9. J-V characteristics for optimal thickness of perovskite layer

parameters determining the PV performance. For example, during the summer time solar panels are often exposed to very high amount of heat and their temperature can rise as high as 70–80°C, and, as a result, the performance parameters decrease. In the present study the temperature effect was analyzed in the range of 300–360 K (27–87°C).

In PV devices working in elevated temperatures the open-circuit voltage is the most affected parameter. This effect is also visible in the case of the examined PSC structures. The estimated V_{oc} voltage drop temperature coefficients are approximately equal 2.03 mV/°C, 1.80 mV/°C and 1.78 mV/°C for PSC with TiO_2, SnO_2 and ZnO as the ETL, respectively. In contrary, the short-circuit current densities remain practically unchanged for the whole range of the temperature. The effect of temperature on J-V characteristic for the best performing PCS model with the SnO_2 ETL is presented in Fig. 10. Fig. 11 shows the effect of temperature on output power for the same system. It is clearly seen that maximum power point is shifted towards lower voltages and the power conversion energy parameter is worsening, when the operating temperature increases.

Conclusion

The main challenge in photovoltaic solar cell designing is to maximize the efficiency to cost ratio. Numerical simulation is a powerful tool allowing the insight into the physics of the PV device and to analyze the impact of various factors on the overall performance. It is obvious that the simulation work

Table 1. Input parameters for the simulations [5, 6]

Parameter	CuI	$CH_3NH_3PbI_3$	TiO_2	SnO_2	ZnO
Band gap [eV]	3.10	1.56	3.26	3.60	3.20
Electron affinity [eV]	2.10	3.90	4.20	3.93	4.10
Dielectric permittivity	6.5	10.0	10.0	8.0	8.1
CB effective density of states [1/cm^3]	2.2 E+19	2.7 E+18	2.5 E+18	3.16 E+18	4.5 E+18
VB effective density of states [1/cm^3]	1.8 E+19	3.9 E+18	1.0 E+18	2.5 E+19	1.0 E+18
Electron mobility [cm^2/Vs]	10.0	15.0	0.1	15.0	300.0
Hole mobility [cm^2/Vs]	43.9	15.0	0.1	0.1	1.0
Shallow donor density N_d [1/cm^3]	0	0	1.0 E+19	1.0 E+19	1.0 E+19
Shallow acceptor density N_a [1/cm^3]	1.0E+19	1.0 E+11	0	0	0
Total bulk defect density N_t [1/cm^3]	1.0 E+17	1.5 E+16	1.0 E+17	1.0 E+17	1.0 E+17

Table 2. Performance parameters of optimized perovskite solar cells

	ETL	Thickness [µm]	R_S [Ωcm^2]	R_{SH} [Ωcm^2]	V_{oc} [V]	J_{sc} [mA/cm^2]	FF [%]	PCE [%]
Model 1	TiO_2	0.53	8.8	337.0	1.10	22.76	53.44	13.29
		0.55	3.0	4250.0	1.10	23.51	65.87	17.08
Model 2	SnO_2	0.43	8.8	337.0	1.12	21.95	57.85	14.29
		0.43	3.0	4250.0	1.13	22.53	71.86	18.33
Model 3	ZnO	0.47	8.8	337.0	1.10	22.19	55.72	13.66
		0.47	3.0	4250.0	1.11	22.77	69.12	17.53

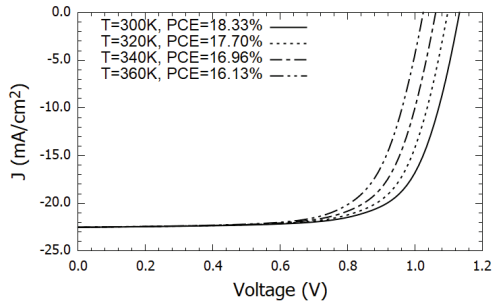

Fig. 10. J-V characteristics as a function of operating temperature for the solar cell with the SnO_2 electron-transport layer

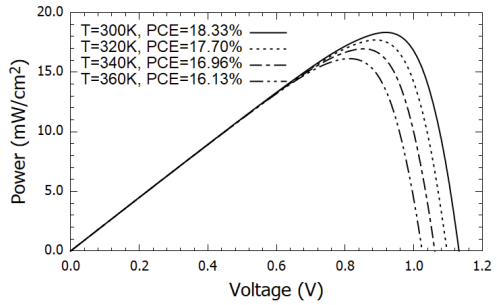

Fig. 11. Output power as a function of operating temperature for the solar cell with the SnO_2 electron-transport layer

reduces the unnecessary costs and enables to optimize the solar cell performance.

In this study the thin-layer lead-halide perovskite solar cell was investigated by the use of the SCAPS-1D simulation method [2, 3]. Three model structures were chosen for the examination, that is, $CuI/CH_3NH_3PbI_3/TiO_2$ (Model 1), $CuI/CH_3NH_3PbI_3/SnO_2$ (Model 2) and $CuI/CH_3NH_3PbI_3/ZnO$ (Model 3) and the input parameters were carefully selected to make the models as realistic as possible. The perovskite layer thickness was optimized for all the systems. The detailed analysis of the power conversion efficiency (PCE), fill factor (FF), open-circuit voltage (V_{oc}), short-circuit current (J_{sc}) and output power at various operating temperatures indicates that the best performance could be achieved for the system with SnO_2 as a electron-transport layer (Model 2).

***Authors**: Maciej Łuszczek, Grzegorz Łuszczek, Dariusz Świsulski, Faculty of Electrical and Control Engineering, Gdańsk University of Technology, str. Gabriela Narutowicza 11/12, 80-233 Gdańsk, Poland.*
E-mail: maciej.luszczek@pg.edu.pl

REFERENCES

[1] Bahers T. L., Rerat M., Sautet P., Semiconductors used in photovoltaic and photocatalytic devices: assessing fundamental properties from DFT, *The Journal of Physical Chemistry C*, 118 (2014), 5997–6008, DOI: 10.1021/jp409724c
[2] Burgelman M., Nollet P. , Degrave S., Modelling polycrystalline semiconductor solar cells, *Thin Solid Films*, 361–362 (2000), 527–532, DOI: 10.1016/S0040-6090(99)00825-1
[3] Burgelman M. , Decock K., Khelifi S., Abass A., Advanced electrical simulation of thin film solar cells, *Thin Solid Films*, 535 (2013), 296–301, DOI: 10.1016/j.tsf.2012.10.032
[4] Moghadamzadeh S., Hossain I.M., Jakoby M., Nejand B.A., Rueda-Delgado D., Schwenzer J.A., Gharibzadeh S., Abzieher T., Khan M.R., Haghighirad A.A., Howard I.A., Richards B.S., Lemmerabd U., Paetzold U.W., Spontaneous enhancement of the stable power conversion efficiency in perovskite solar cells, *J. Mater. Chem. A*, 8 (2020), 670–682, DOI: 10.1039/c9ta09584e
[5] Mandadapu U., Vedanayakam S.V., Thyagarajan K. , Babu B.J., Optimisation of high efficiency tin halide perovskite solar cells using SCAPS-1D, *Int. J. Simulation and Process Modelling*, 13 (2018), No.3, 221–227, DOI: 10.1504/IJSPM.2018.10014179
[6] Rahman S., Miah S., Marma M.S. W., Sabrinax T., Simulation based investigation of inverted planar perovskite solar cell with all metal oxide inorganic transport layers, *2019 International Conference on Electrical, Computer and Communication Engineering (ECCE), IEEE Xplore* (2019), DOI: 10.1109/ECACE.2019.8679283
[7] Lee J., Baik S., Enhanced crystallinity of $CH_3NH_3PbI_3$ by the precoordination of PbI_2–DMSO powders for highly reproducible and efficient planar heterojunction perovskite solar cells, *RSC Adv.*, 8 (2018), 1005–1013, DOI: 10.1039/c7ra12304c
[8] Nishi K., Oku T., Kishimoto T., Ueoka N., Suzuki A., Photovoltaic characteristics of $CH_3NH_3PbI_3$ perovskite solar cells added with ethylammonium bromide and formamidinium iodide, *Coatings*, 10 (2020), 410–419, DOI: 10.3390/coatings10040410